Electronic supplementary information

N,N-diethylamine appended binuclear Zn(II) complexes; Highly selective and sensitive fluorescent chemosensors for picric acid

Amit Kumar, Ashish Kumar and Daya Shankar Pandey*

Department of Chemistry, Faculty of Science, Banaras Hindu University Varanasi 221 005 India

Contents:

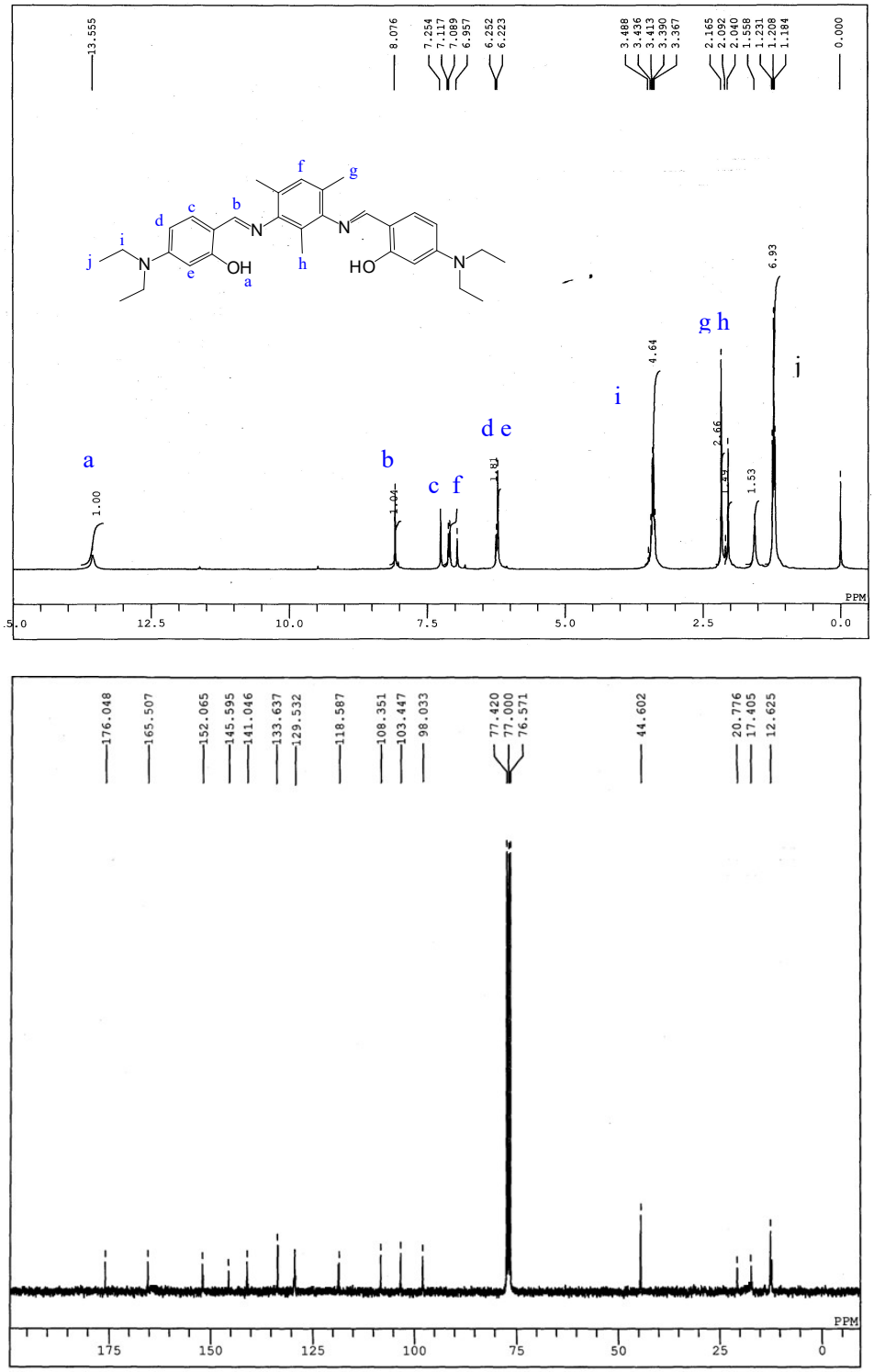

Fig. S1 ^{1}H (top) and ^{13}C NMR (bottom) spectra of $\mathbf{H_2L^1}$.

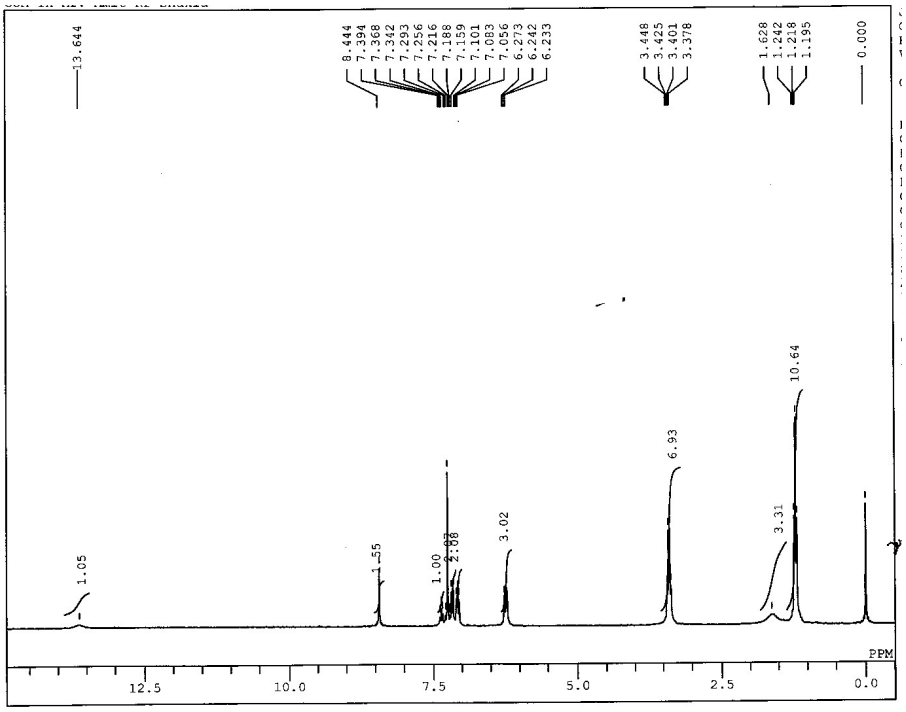

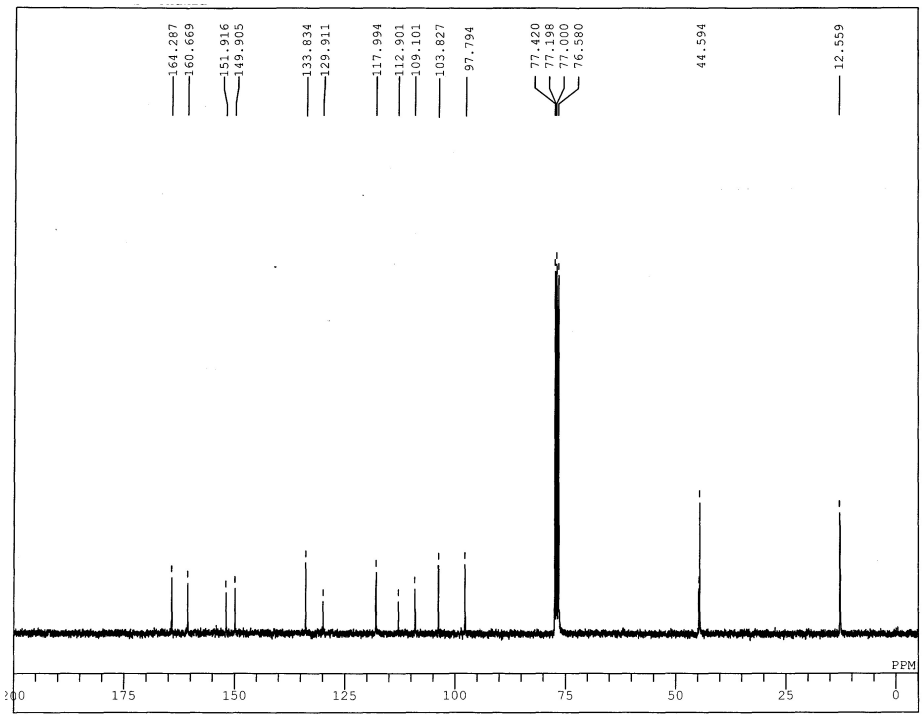

Fig. S2 ^{1}H (top) and ^{13}C NMR (bottom) spectra of $\mathbf{H_2L^2}$.

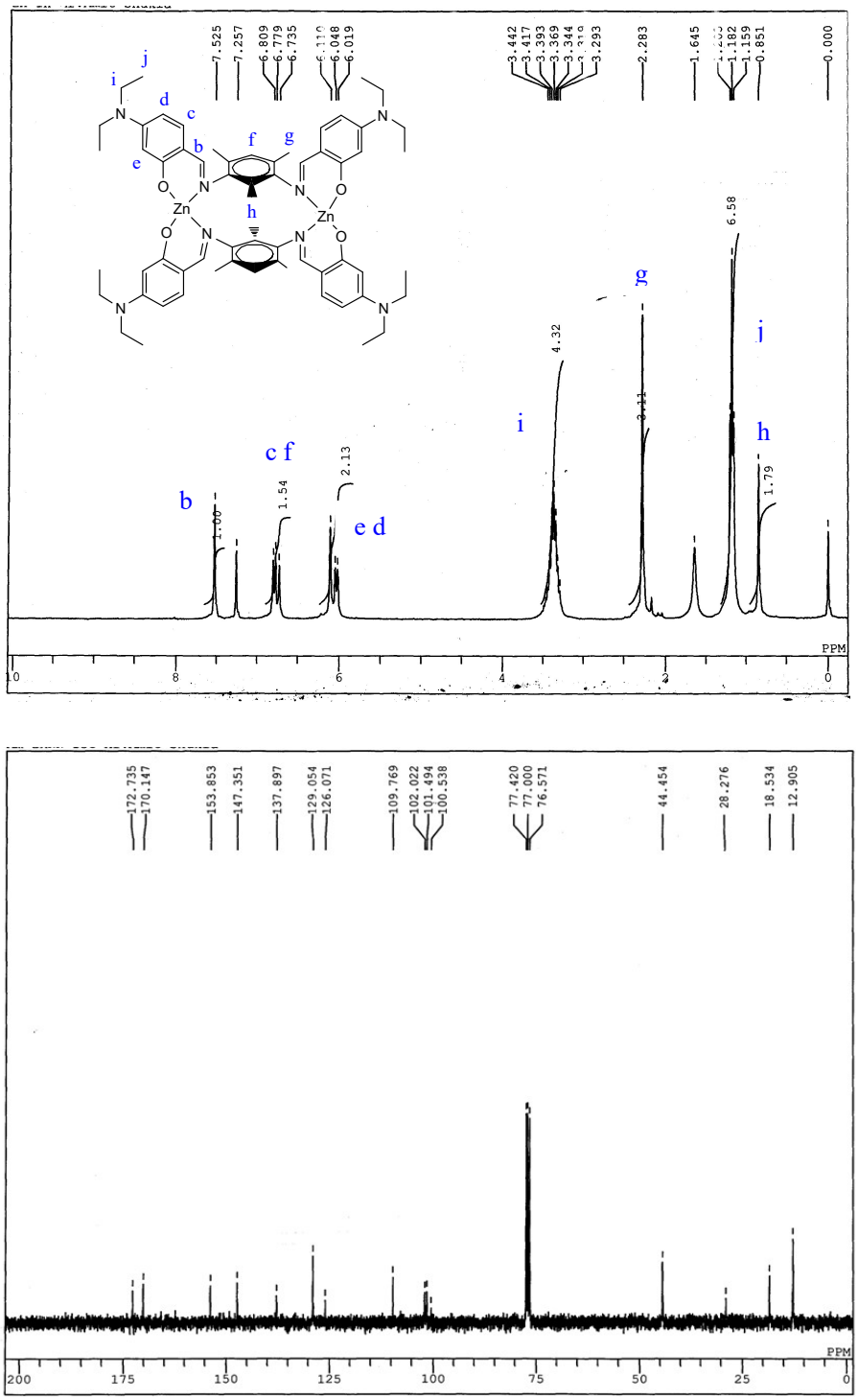

Fig. S3 ^{1}H (top) and ^{13}C NMR (bottom) spectra of **1**.

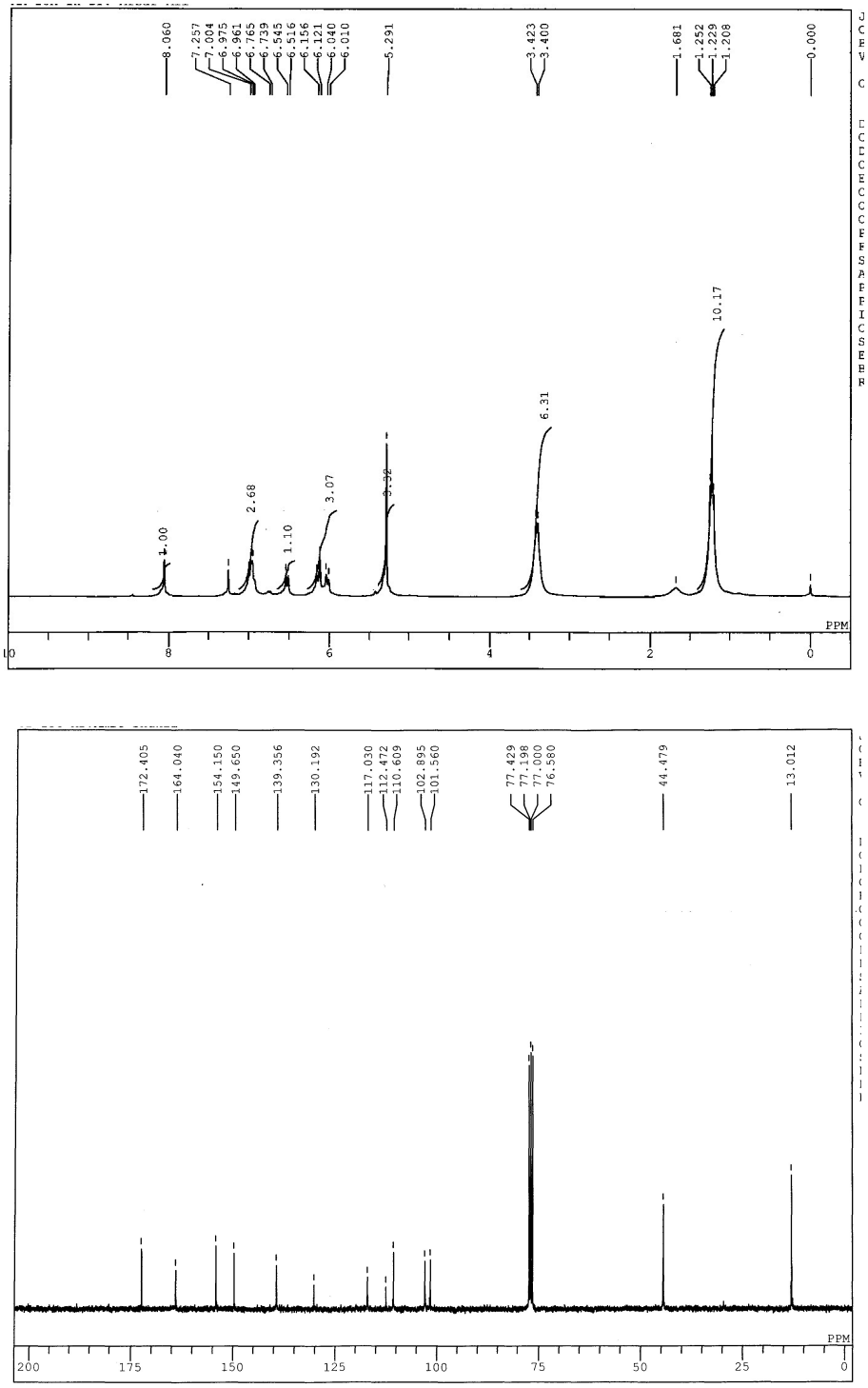

Fig. S4 ^{1}H (top) and ^{13}C NMR (bottom) spectra of **2**.

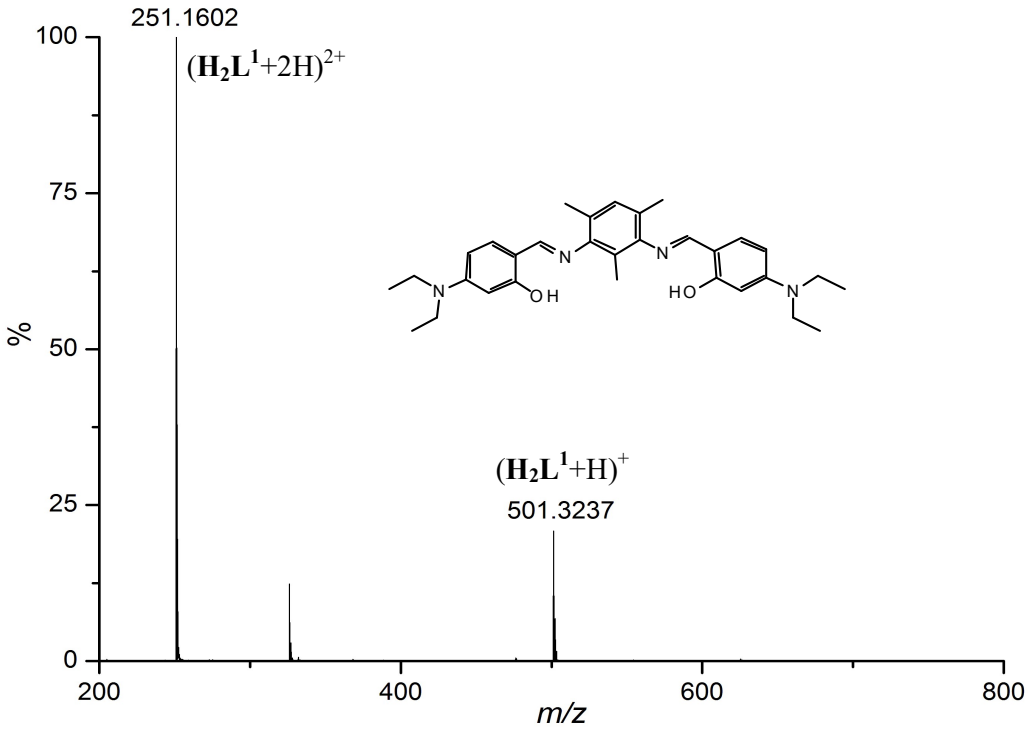

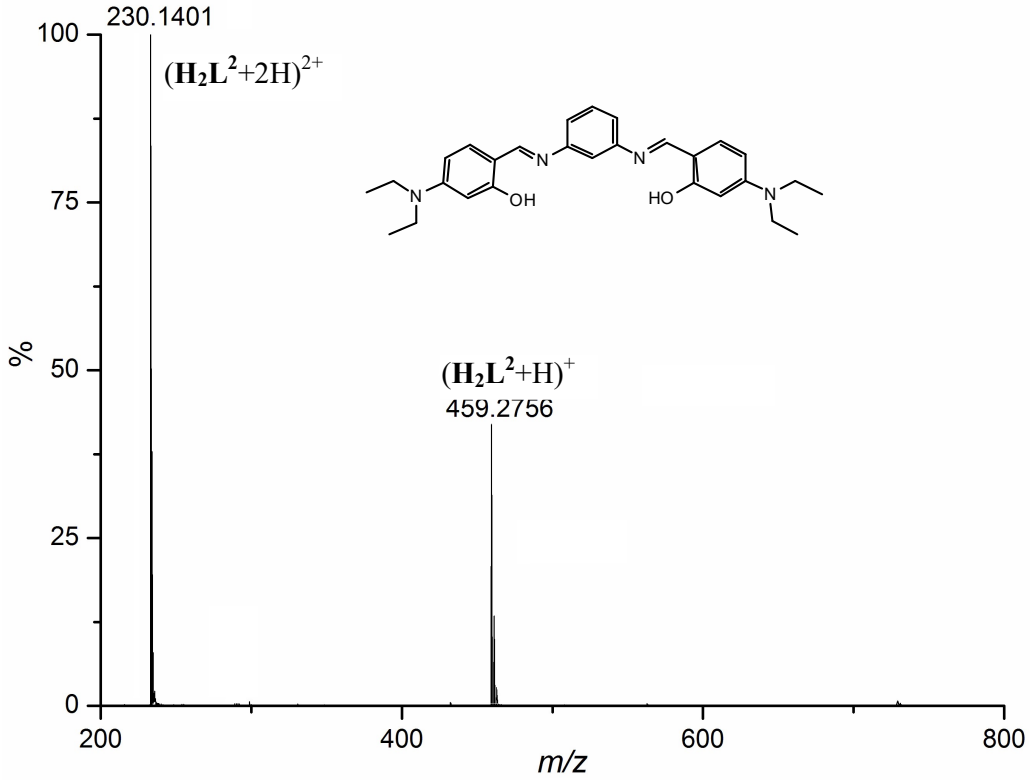

Fig. S5 ESI-MS of $\mathbf{H_2L^1}$ (to) and $\mathbf{H_2L^2}$ (bottom).

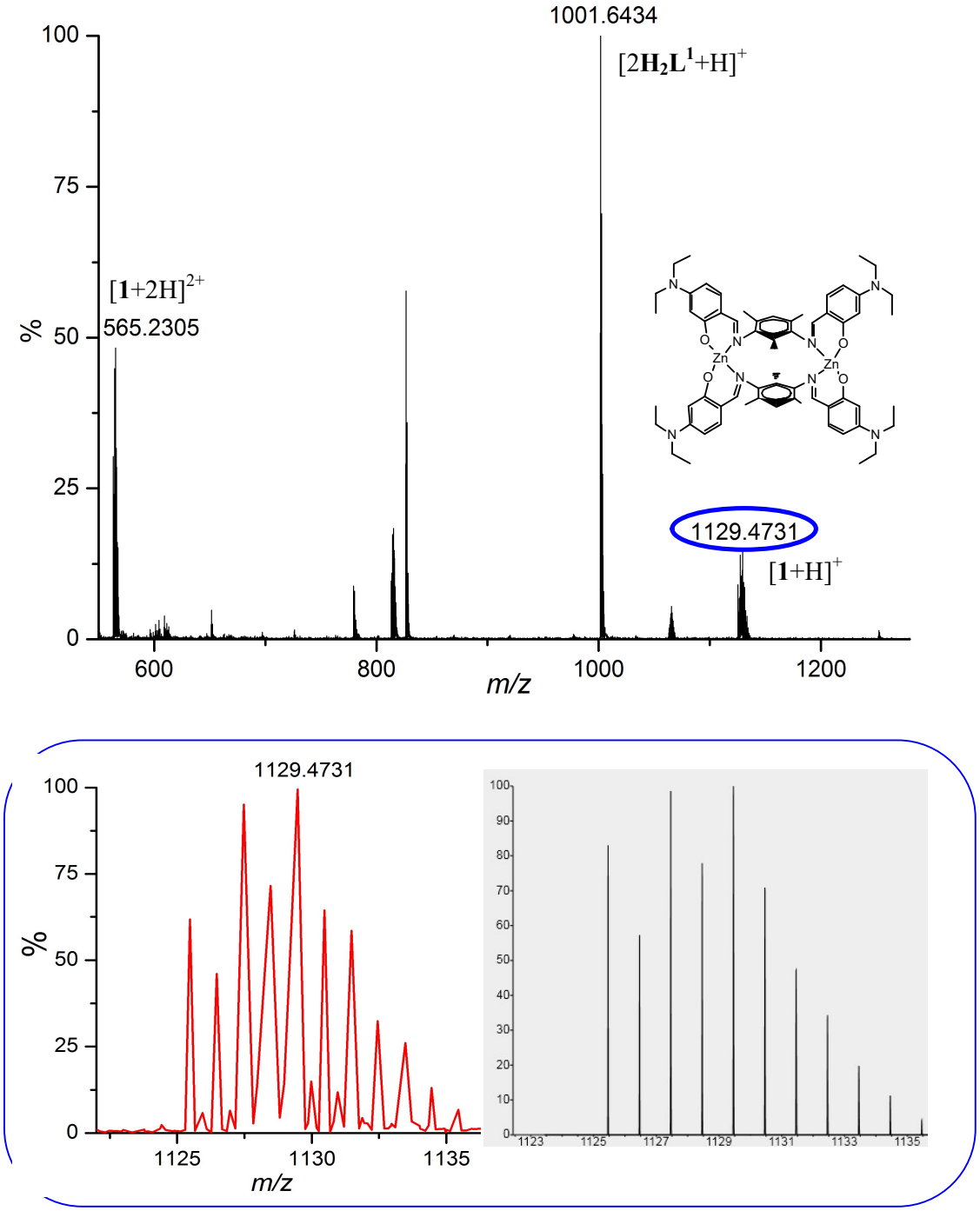

Fig. S6 ESI-MS of **1** (top) and simulated isotopic pattern for molecular ion peak at *m/z* 1129.4731 (bottom).

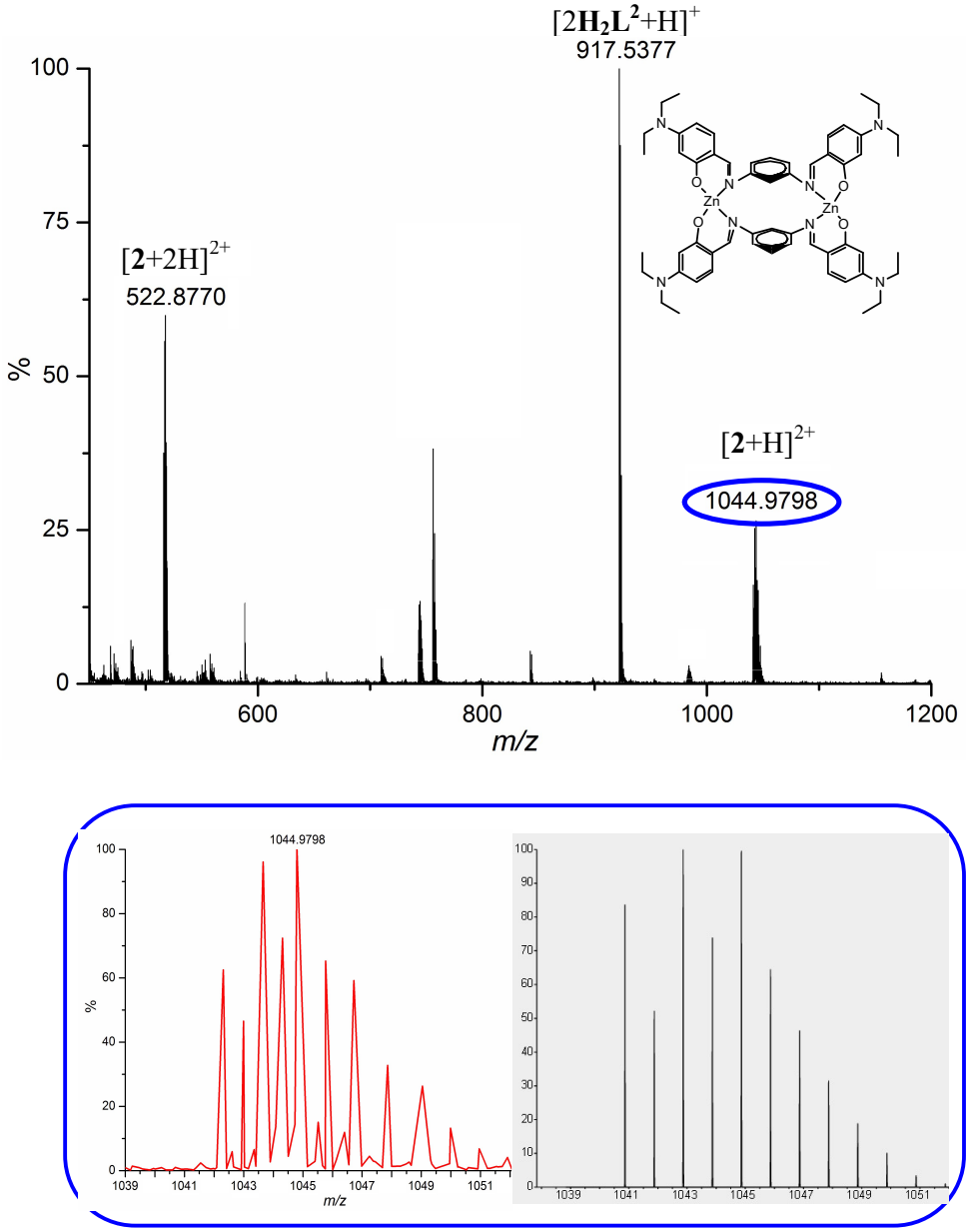

Fig. S7 ESI-MS of **2** (top) and simulated isotopic pattern for the molecular ion peak at *m/z* 1044.9798 (bottom).

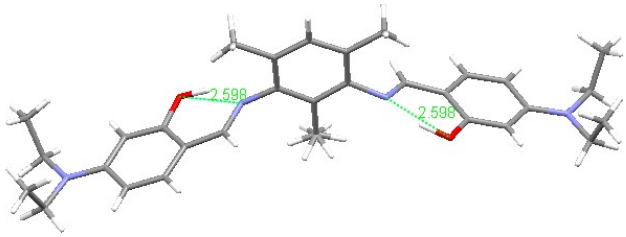

Fig. S8 Intramolecular hydrogen bonding interactions in $\mathbf{H_2L^1}$.

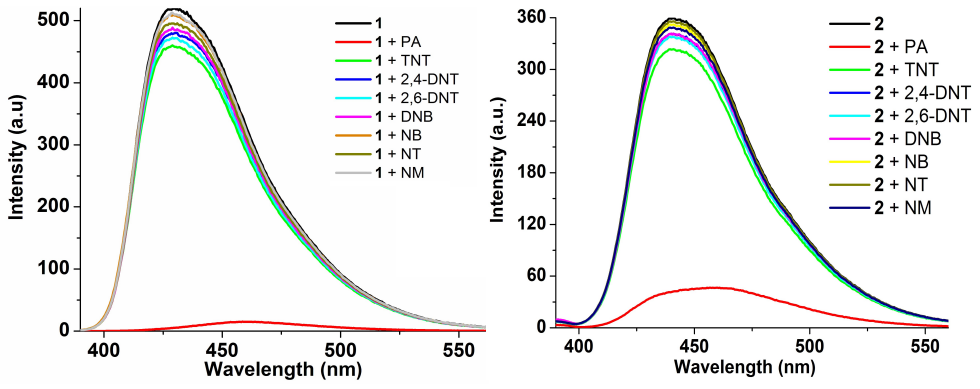

Fig. S9 Fluorescence Spectra of **1** and **2** (c, 1 μM in CH_3CN) in presence of 14 equiv of various NECs.

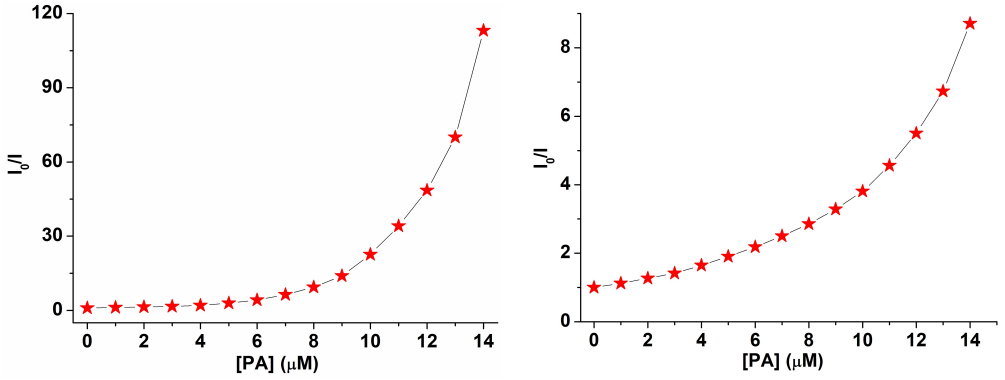

Fig. **S10** Nonlinear SV plot for **1** and **2** with varying amount of PA.

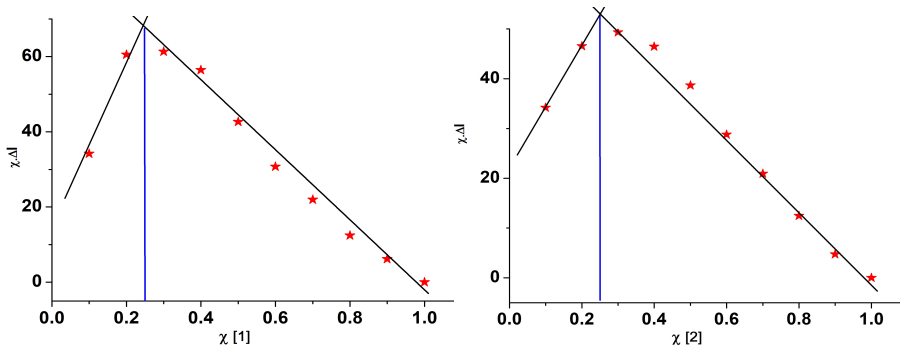

Fig. **S11** Job′s plot analysis showed 1:4 binding ratio between **1** and PA.

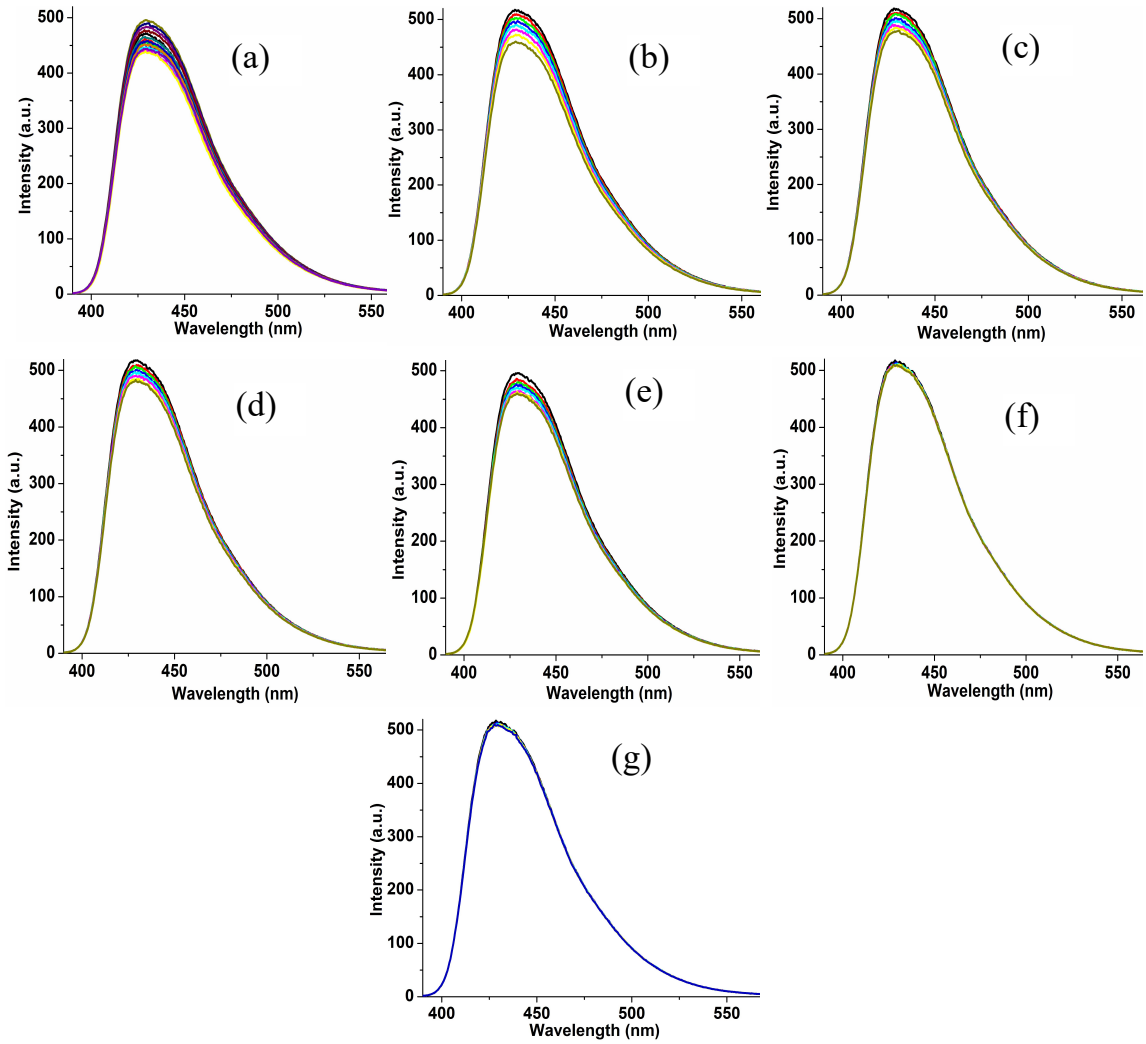

Fig. **S12** Fluorescence spectra of **1** (c, 1 μM in CH_3CN) showing quenching with increasing amounts (0.0-14.0 equiv) of various NECs [TNT (a), 2,4-DNT (b), 2,6-DNT (c), DNB (d), 4-NT (e), 4-NB (f), 4-NM (g)] upon excitation at 378 nm.

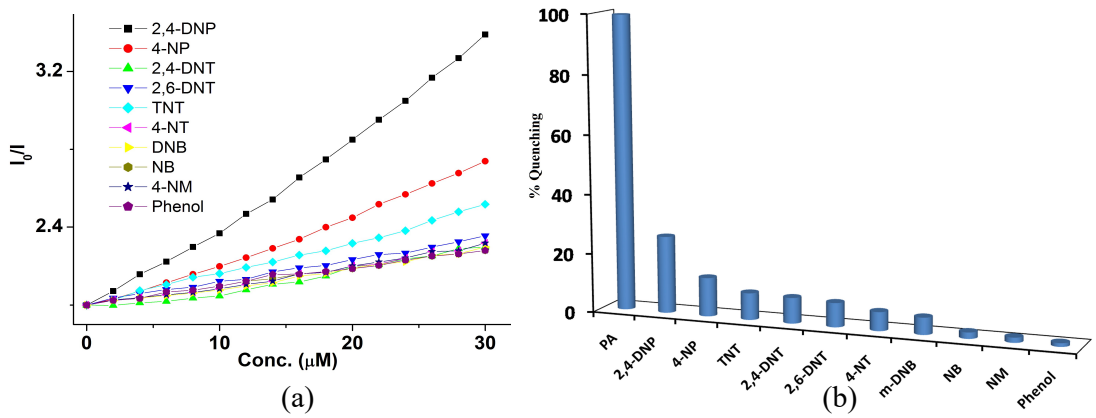

Fig. **S13** SV plot (a) and percentage fluorescence quenching graph (b) for **1** (c, 1 μM in CH_3CN) in presence of 14 equiv. of various NECs (2,4-DNP, 4-NP, TNT, 2,4-DNT, 2,6-DNT, DNB, 4-NT, 4-NB, 4-NM, phenol).

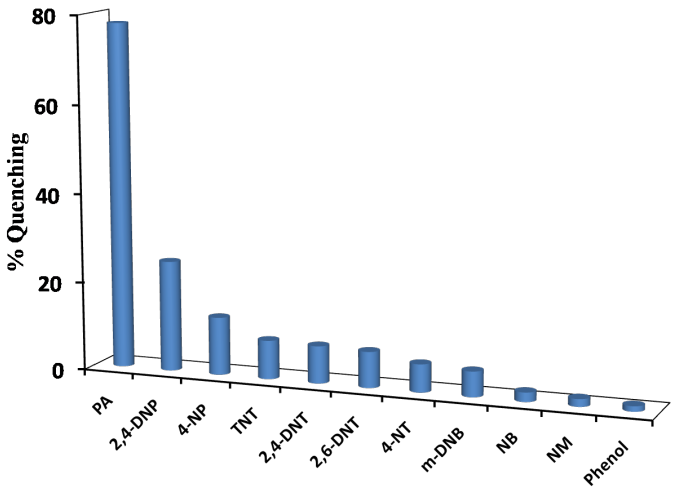

Fig. **S14** Percentage fluorescence quenching graph for **2** in presence of various NECs (2,4-DNP, 4-NP, TNT, 2,4-DNT, 2,6-DNT, DNB, 4-NT, 4-NB, 4-NM, phenol).

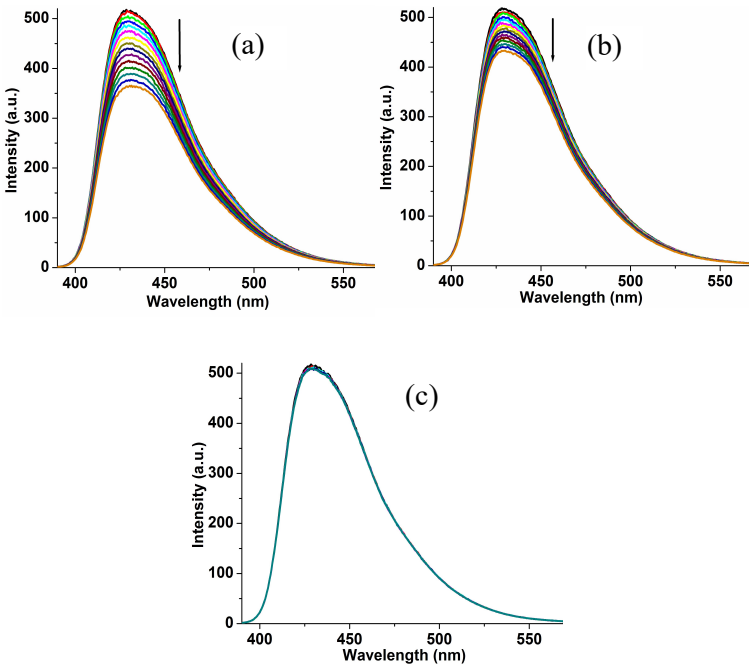

Fig. **S15** Fluorescence quenching spectra of **1** (c, 1 μM in CH_3CN) with increasing amounts (0.0-14.0 equiv) of 4-DNP (a), 4-NP (b) and phenol (c) upon excitation at 378 nm.

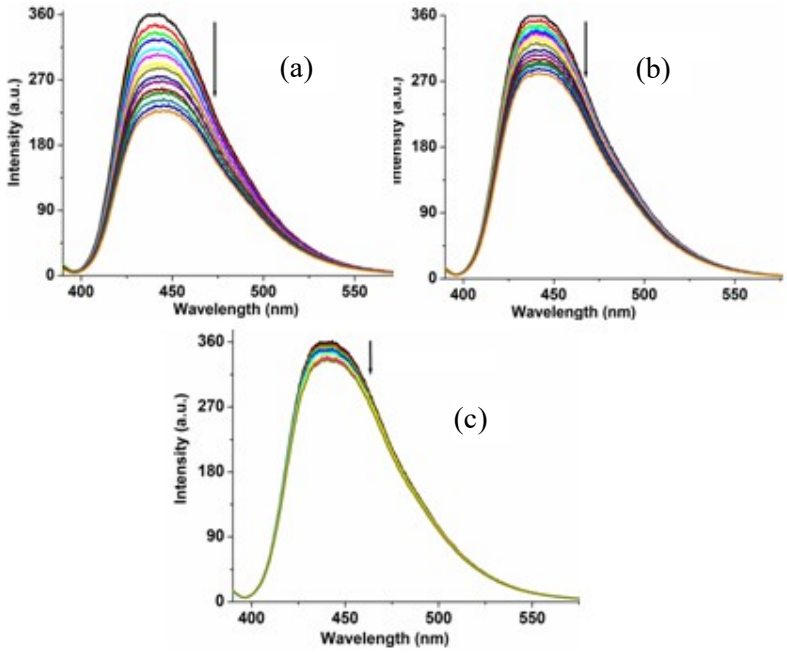

Fig. **S16** Fluorescence quenching spectra of **2** (c, 1 μM in CH_3CN) with increasing amounts (0.0-14.0 equiv) of 4-DNP (a), 4-NP (b) and phenol (c) upon excitation at 390 nm.

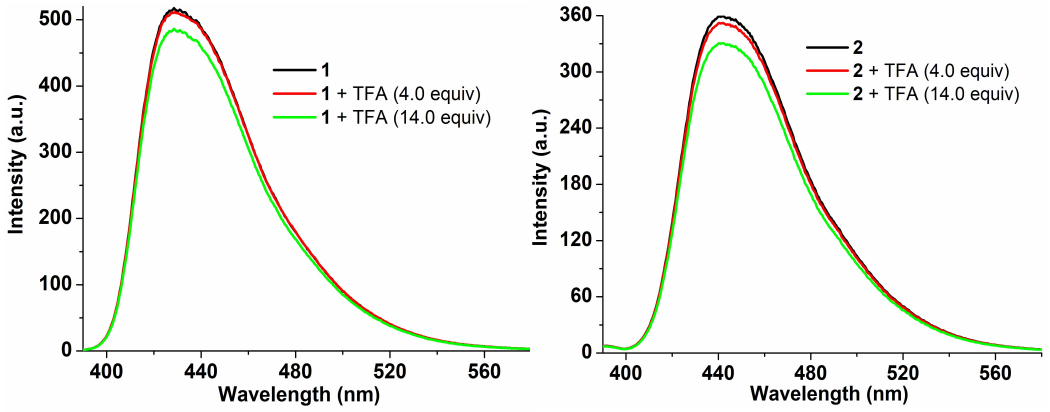

Fig. **S17** Fluorescence spectra of **1** and **2** (c, 1 μM in CH_3CN) in presence of TFA (4 equiv).

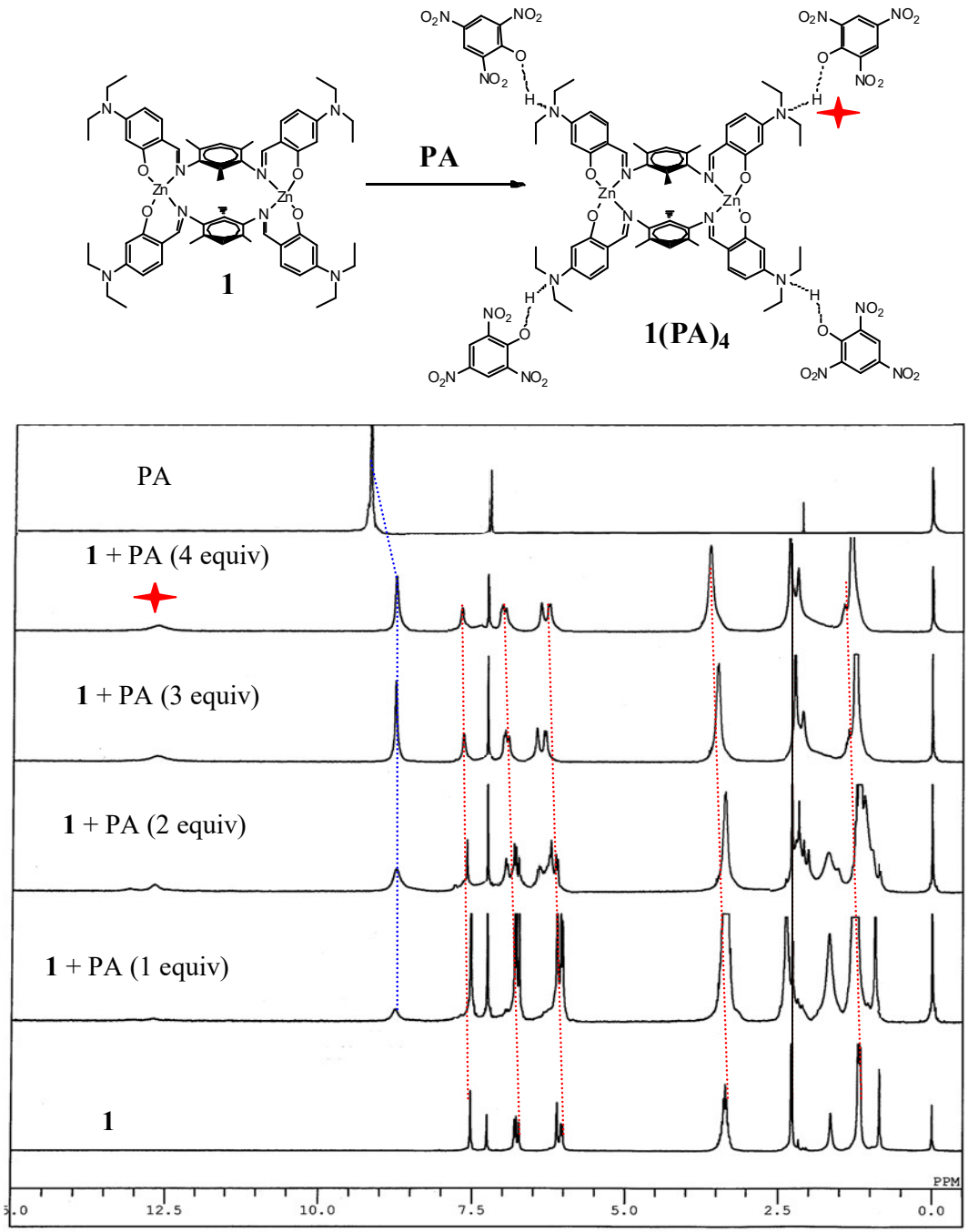

Fig. **S18** ^{1}H NMR titration spectra of **1** in presence of varying amount of PA in $CDCl_3$ [red lines represent downfield shift in aromatic and aliphatic protons in **1**, blue line presents the appearance of picric acid proton and red star shows the formation of $(CH_3CH_2)_2N\underline{H}^+$ resulted by the protonation of N,N-diethyl amine nitrogen.

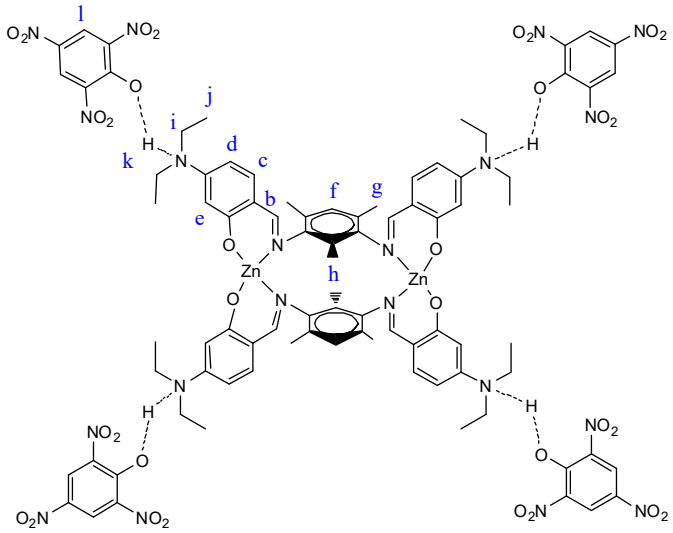

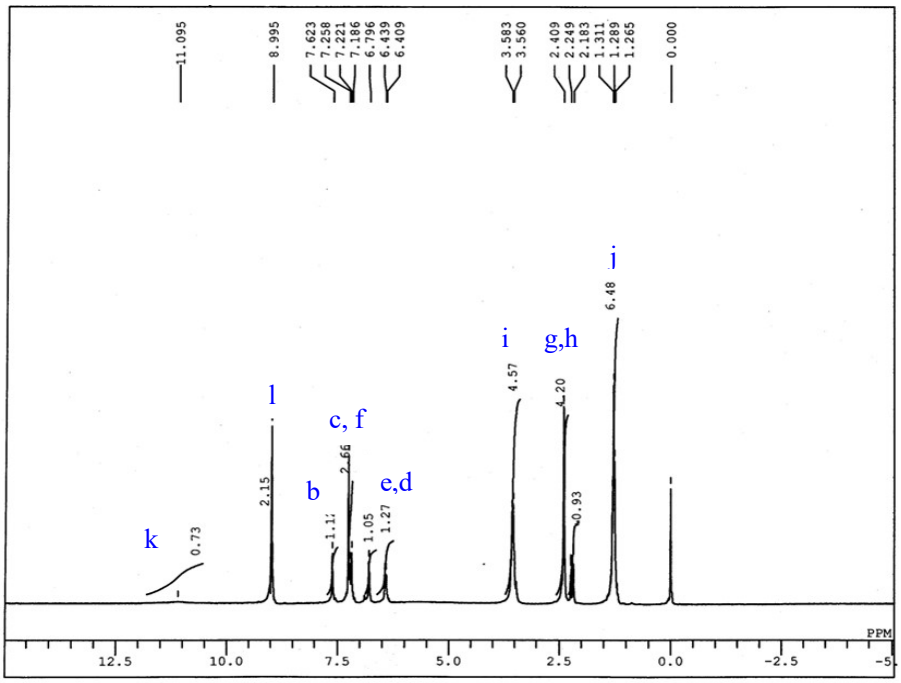

Fig. **S19** ^{1}H NMR spectra of the ensuing species **1.**$(PA)_4$ in $CDCl_3$.

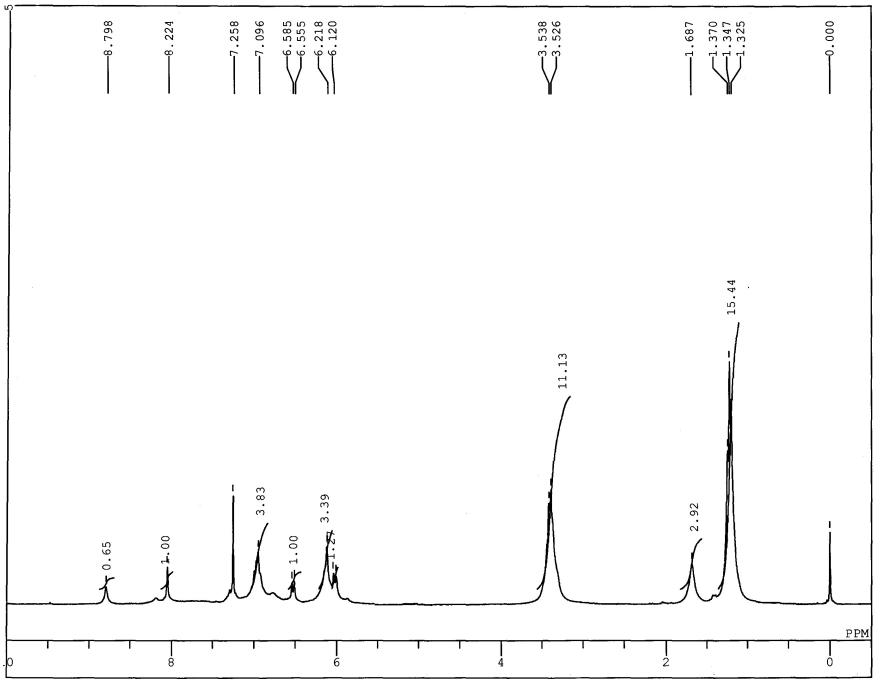

Fig. **S20** ^{1}H NMR spectra of the ensuing species **2**.$(PA)_4$ in $CDCl_3$.

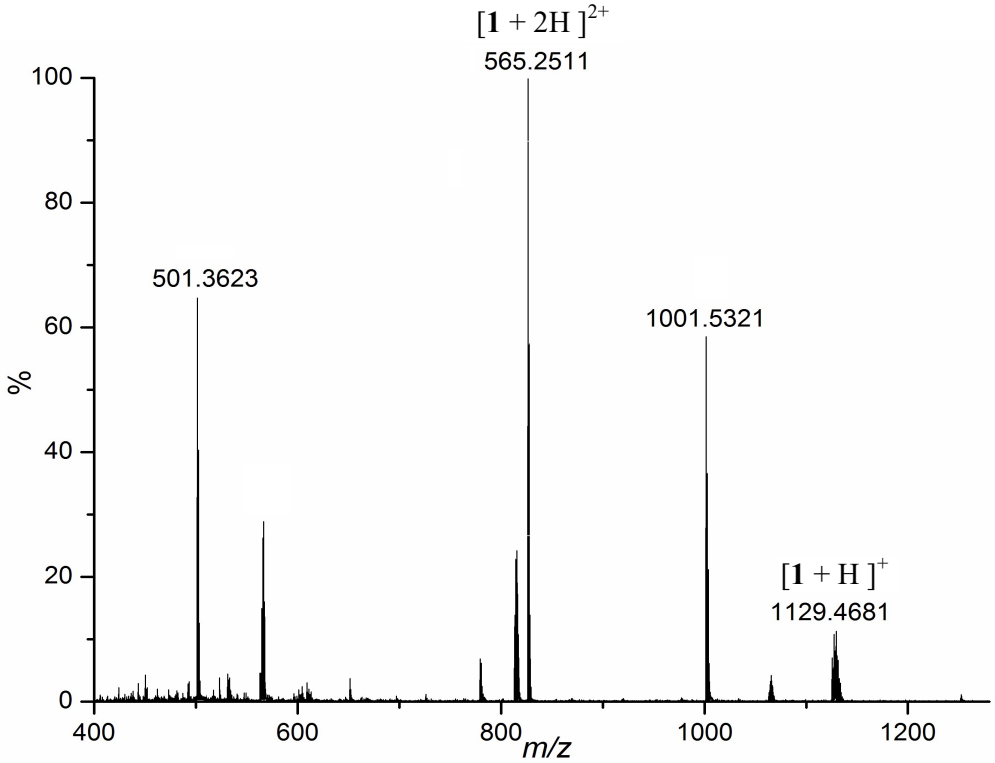

Fig. **S21** ESI-MS of the ensuing species **1**.$(PA)_4$.

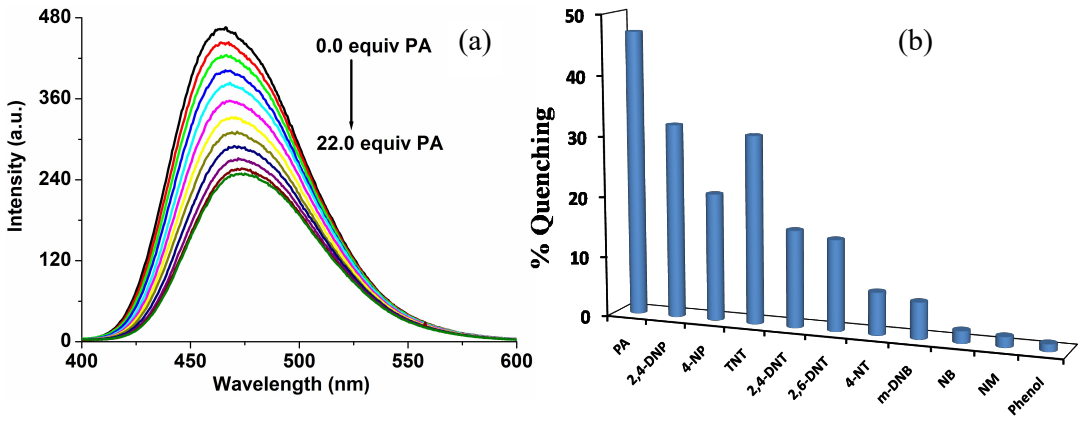

Fig. **S22** Fluorescence quenching spectra of **M** with increasing amounts of PA (a) and percentage fluorescence quenching graph in presence of various NECs (2,4-DNP, 4-NP, TNT, 2,4-DNT, 2,6-DNT, DNB, 4-NT, 4-NB, 4-NM, phenol).

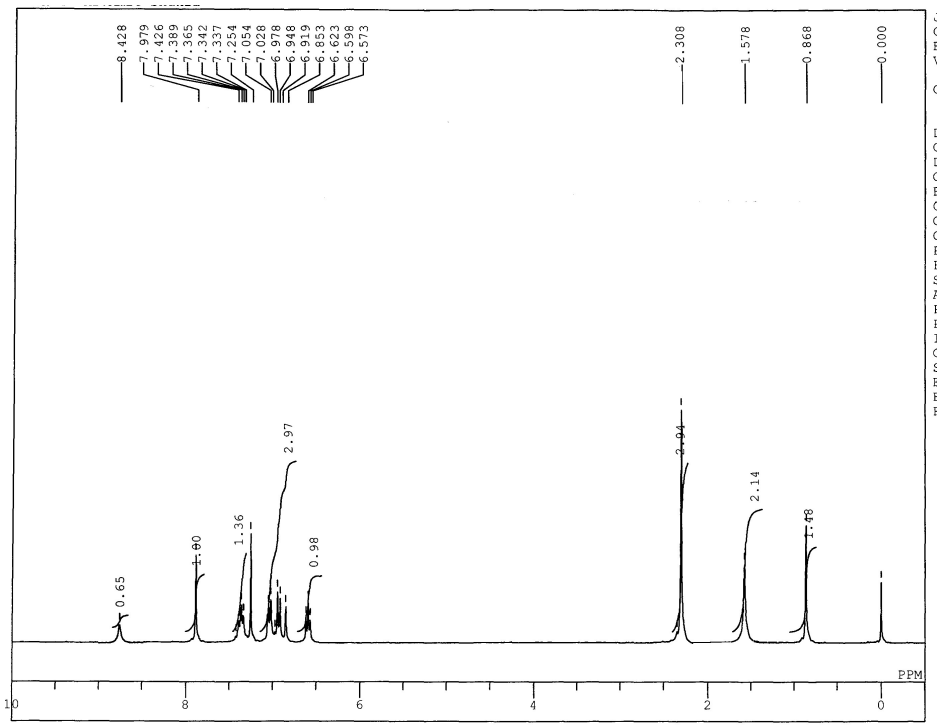

Fig. **S23** ^{1}H NMR spectra of **M** in presence of PA (4.0 equiv).

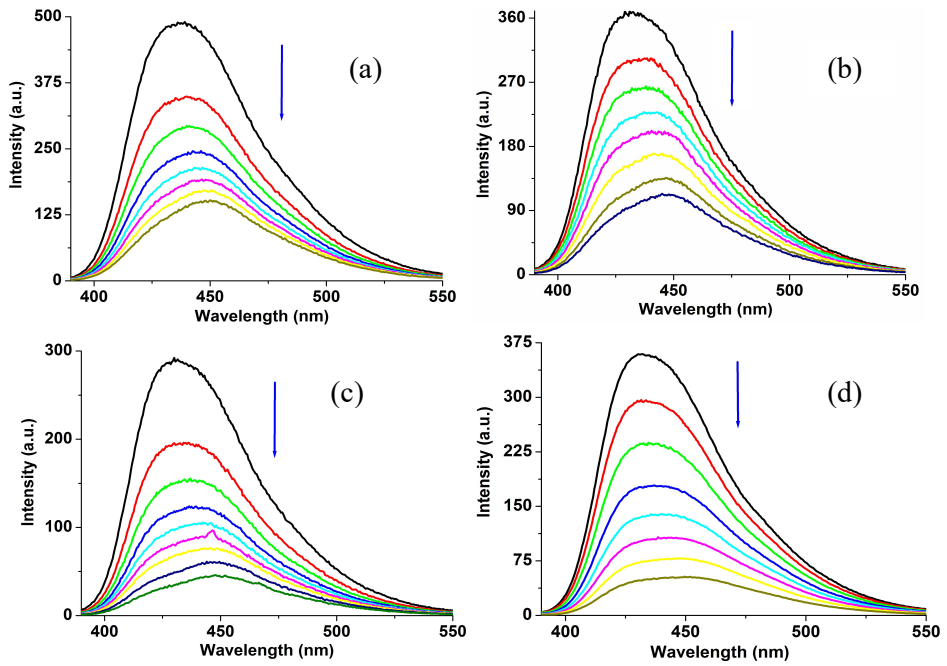

Fig. **S24** Fluorescence quenching spectra of **1** (c, 1 μM) with increasing amounts of PA (0.0-14.0 equiv) in different solvents CH_2Cl_2 (a), $CHCl_3$ (b), THF (c) and DMSO (d).

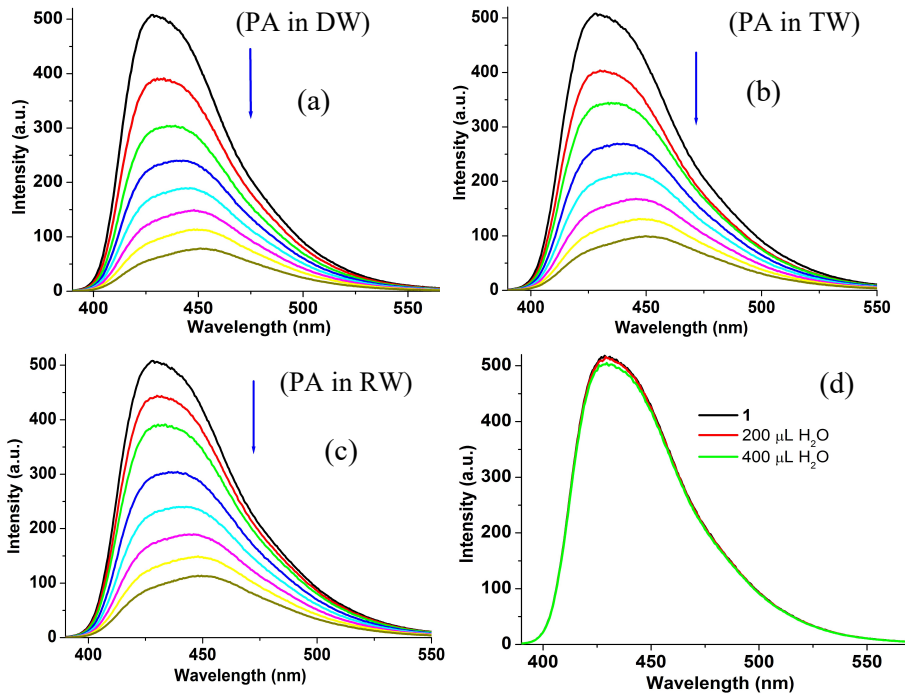

Fig. **S25** Fluorescence quenching spectra of **1** (c, 1 μM in CH_3CN) with increasing amounts of PA (0.0-14.0 equiv) in different water samples [distilled water (a), tap water (b), river water (c)] and in presence of blank water [200–400 μL, (d)].

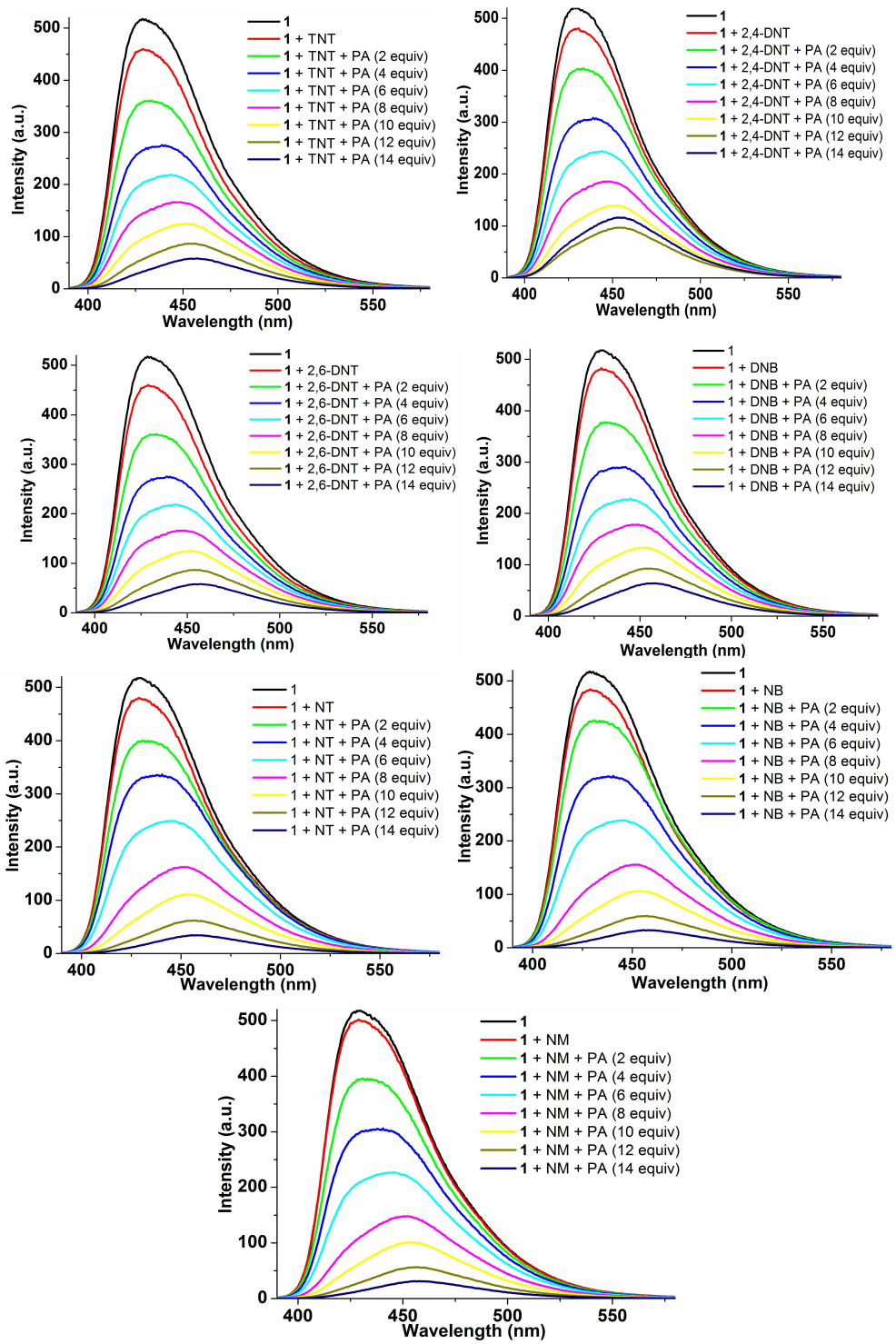

Fig. **S26** Fluorescence spectra of **1** (c, 1 μM in CH_3CN) in presence of various NECs [14 equiv of TNT (a), 2,4-DNT (b), 2,6-DNT (c), DNB (d), 4-NT (e), 4-NB (f), 4-NM (g) (redlines)] followed by the incremental addition of PA.

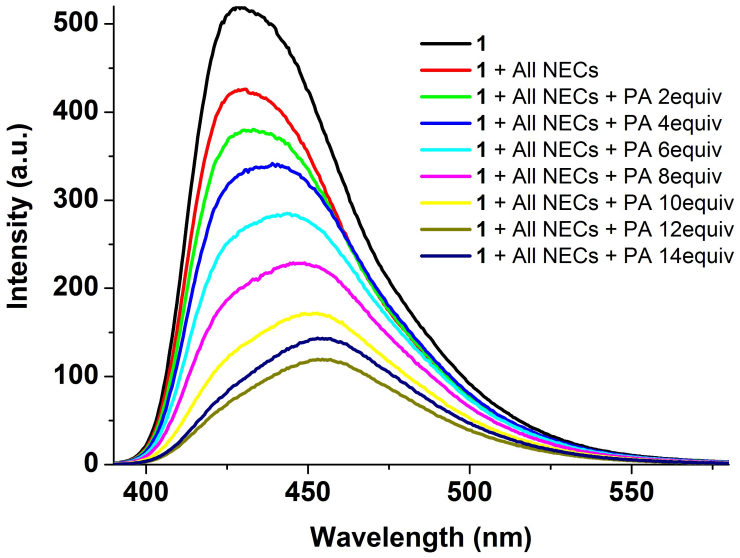

Fig. **S27** Fluorescence spectra of **1** (c, 1 μM in CH_3CN) in simultaneous presence of various NECs [7 × 14 equiv, redline] followed by

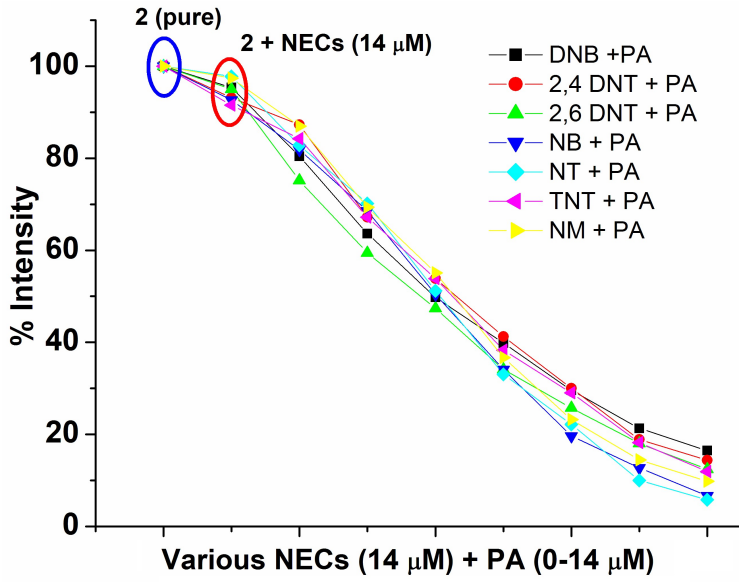

Fig. S28 Changes in % fluorescence intensity of **2** on addition of various NECs followed by PA, [100% intensity for pure **2** (blue circle), and in presence of various NECs without PA (red circle), followed by additions PA (other points)].

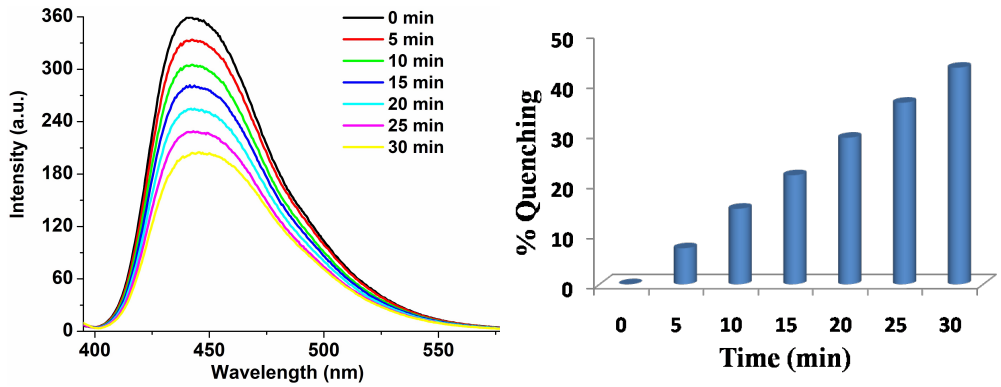

Fig. S29 Fluorescence titration spectra (a) and % fluorescence quenching (b) for **2** (c, 1 μM in CH_3CN) on exposure of vapour of PA at different time intervals (5–30 min).

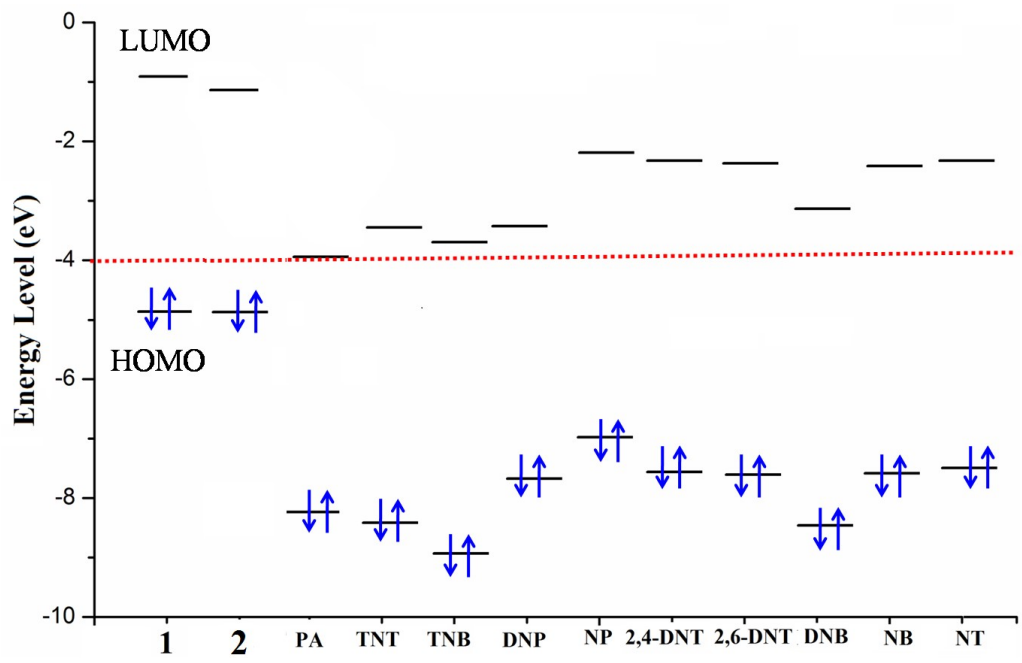

Fig. **S30** Energy level diagram for the frontier molecular orbital (HOMO and LUMO) for the complexes **1**/**2** and various NECs. The HOMO for **1** and **2** showed lower energy than LUMO of NECs and ruled out the GS charge transfer between complexes (without protonation) and NECs.

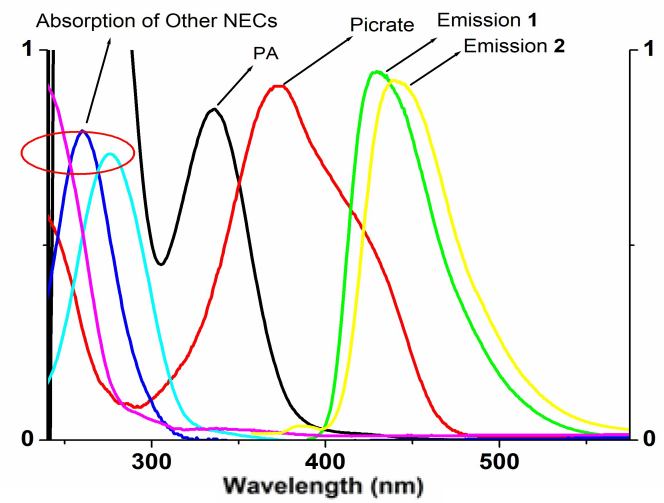

Fig. S31 Spectral overlap between the normalized emission spectrum of **1/2** and normalized absorption spectra of various NECs (a), higher spectral overlap between emission spectra of **1/2** and normalized absorption spectra picrate than PA (b).

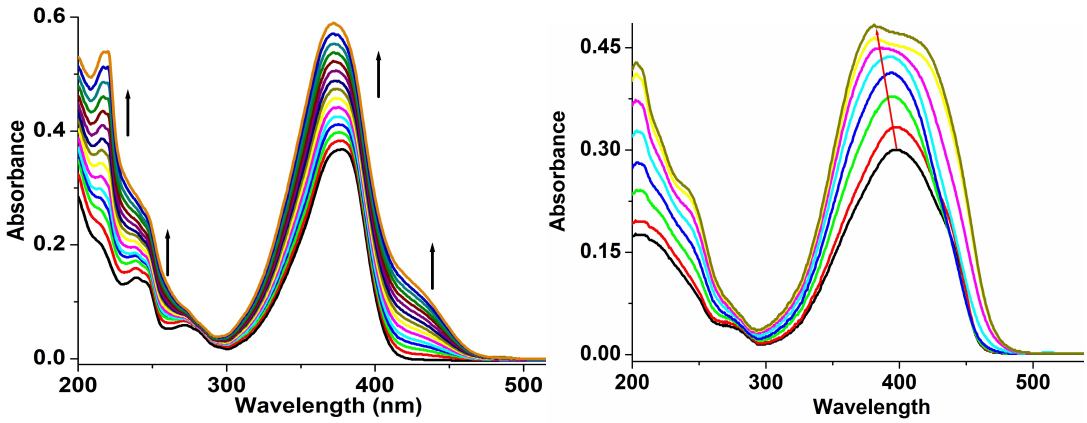

Fig. **S32** UV–vis titration spectra of **1** and **2** (c, 1 μM in CH_3CN) in presence of various amount of PA (14 equiv).

Table S1. Crystallographic parameter of $\mathbf{H_2L^1}$ and **1**.

	$\mathbf{H_2L^1}$	**1**
empirical formula	$C_{31}H_{40}N_4O_2$	$C_{62}H_{76}N_8O_8Zn_2$
formula weight	500.6	1192.09
crystal system	orthorhombic	Monoclinic
space group	*Fdd2*	$P2_1/n$
a (A°)	20.763(3)	13.2334(5)
b (A°)	31.748(5)	16.7995(6)
c (A°)	8.6715(12)	15.3797(6)
α (deg)	90.00	90.00
β (deg)	90.00	103.611(2)
γ (deg)	90.00	90.00
V (A° 3)	5716.3(15)	3323.1(2)
Color and habit	Light Yellow block	Yellow block
Z	8	2
dcal (g/cm^3)	1.164	1.191
Crystalsize (mm^3)	0.18 × 0.16 × 0.12	0.30 × 0.27 × 0.22
Temperature (K)	292(2)	292(2)
wavelength (A°)	MoK\α 0.71073	MoK\α 0.71073
μ (mm^{-1})	0.073	0.776
GOFa on F2	1.108	1.243
final R indices[I > 2σ(I)]	R1 = 0.0321	R1 = 0.0598
	wR2= 0.0865	wR2= 0.1647
R indices (All data)	R1 = 0.0351	R1 = 0.1196
	wR2 = 0.0895	wR2 = 0.1859

Table S2. Selected bond lengths (Å) in $\mathbf{H_2L}$[1] and **1**.

bond distances (Å)			
H_2L		**1**	
O1 C13	1.356(5)	N1 C1	1.440(4))
N1 C7	1.264(6)	N1 C10	1.308(4)
N1 C1	1.423(6)	O1 C12	1.316(4)
N2 C11	1.362(6)	C21 N2	1.299(4)
N2 C16	1.454(8)	O2 C23	1.315(4)
O1 H1A	1.06(6)	Zn1 O1	1.924(3)
		Zn1 N1	1.988(3)
		Zn1 N2	1.998(3)
		Zn1 O2	1.928(3)

Table S3. Selected bond angles (˚) for **1**.

Selected bond angles (˚)	
O1 Zn1 O2	110.77(12)
O1 Zn1 N1	96.64(11)
O2 Zn1 N1	120.52(12)
O1 Zn1 N2	117.66(12)
O2 Zn1 N2	96.33(11)
N1 Zn1 N2	116.31(12)

Table S4. ^{1}H NMR data of **1** and **1**$(PA)_4$.

Protons	signals	$\mathbf{H_2L^1}$ δ (ppm)	**1** δ (ppm)	**1**$(PA)_4$δ (ppm)	Shift
*H*a	(s)	13.55			
*H*b	(s)	8.07	7.52	7.62	0.10 (downfield)
*H*c	(d)	7.10	6.80	7.20	0.40 (downfield)
*H*d	(d)	6.25	6.04	6.42	0.38 (downfield)
*H*e	(s)	6.22	6.10	6.79	0.69 (downfield)
*H*f	(s)	6.95	6.73	7.18	0.45 (downfield)
*H*i	(q)	3.42	3.38	3.57	0.19 (downfield)
*H*j	(t)	1.20	1.18	1.29	0.11 (downfield)
*H*g	(s)	2.16	2.28	2.41	0.13 (downfield)
*H*h	(s)	2.04	0.85	2.18	1.33 (downfield)
Picrate (*H*l)	(s)			8.99	
-NH (*H*k)	(s)			11.09	

Table S5. ^{1}H NMR data of **2** and **2**(PA)$_4$.

Protons	signals	**H_2L^2** δ (ppm)	**2** δ (ppm)	**1**(PA)$_4$ δ (ppm)	Shift
*H*a	(s)	13.64			
*H*b	(s)	8.44	8.06	8.22	0.16 (downfield)
*H*c	(d)	7.35	6.97	7.09	0.12 (downfield)
*H*d	(d)	7.27	6.02	6.12	0.10 (downfield)
*H*e	(s)	6.23	6.53	6.75	0.22 (downfield)
*H*f	(s)	7.08	6.75	7.18	0.38 (downfield)
*H*i	(q)	3.41	3.41	3.53	0.12 (downfield)
*H*j	(t)	1.21	1.23	1.35	0.12 (downfield)
Picrate (*H*l)	(s)			8.80	